Macromolecules

ARTICLE

pubs.acs.org/Macromolecules

Development of Filler Structure in Colloidal Silica−Polymer Nanocomposites

Jeffrey S. Meth,*[,†] Stephen G. Zane,[†] Changzai Chi,[†] J. David Londono,[†] Barbara A. Wood,[†] Patricia Cotts,[†] Mimi Keating,[†] William Guise,[†] and Steven Weigand[‡]

[†]DuPont Nanocomposite Technologies and DuPont Central Corporate Analytical Services, Central Research & Development, E.I. DuPont de Nemours & Co., Inc., Wilmington, Delaware 19880, United States

[‡]DND-CAT Synchrotron Research Center, Northwestern University, APS/ANL Building 432-A004, 9700 South Cass Avenue, Argonne, Illinois 60439, United States

ABSTRACT: The realization of the full potential for polymeric nanocomposites to manifest their entitled property improvements relies, for some properties, on the ability to achieve maximum particle−matrix interfacial area. Well-dispersed nanocomposites incorporating colloidal silica as the filler can be realized in both polystyrene and poly(methyl methacrylate) matrices by exploiting the charge stabilized nature of silica in nonaqueous solvents which act as Bronsted bases. We demonstrate that dispersions of colloidal silica in dimethylformamide are charge stabilized, regardless of organosilyl surface functionalization. When formulated with polymer solutions, the charge stabilized structure is maintained during drying until the charged double layer collapses. Although particles are free to diffuse and cluster after this neutralization, increased matrix viscosity retards the kinetics. We demonstrate how high molecular weight polymers assist in immobilizing the structure of the silica to produce well-dispersed composites. The glass transition temperatures of these composites do not vary, even at loadings up to 50 vol %.

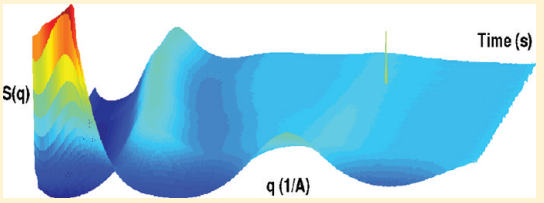

INTRODUCTION

Polymeric nanocomposites (PNCs) hold great promise for improving properties of materials.[1−4] To realize property enhancements, it is necessary to control the dispersion of the particles within the matrix. Controlling the dispersion of the filler particles can be challenging. There have been some efforts to enumerate strategies for controlling dispersion,[5] but there is still a need for a better understanding of how particle structure develops during solvent processing. In general, one wants to achieve one of two structural outcomes when making a nanocomposite. For some goals, one wishes to have the filler dispersed to a full extent, such that interfacial area is maximized. This may be beneficial for mechanical reinforcement in tension, improved fracture toughness, and maximizing transparency. In addition, such high surface area means that a large fraction of the polymeric phase is perturbed, and so the dynamical properties of the resulting composites may show interesting effects attributable to the nanoscopic structure. For other goals, one wishes to create a network, a fractal aggregate of filler particles, to express some critical property such as electrical conductivity or resistance to compressive stress.

In this work, colloidal silica was used as the nanoparticle for several reasons.[6] Its spherical shape, and low polydispersity, enabled us to quantify X-ray scattering. Its relatively low cost means that it could be used in industrial applications. Colloidal silica dispersions can be stabilized solely by charge stabilization. This charge stabilization can be realized in organic as well as aqueous solvents. Gapinski has shown that charge stabilization occurs in dimethylformamide (DMF).[7,8] In DMF, the acidic proton of the silanol surface group hydrolyzes and associates with the oxygen atom of DMF, creating a charged iminium.[9]

PNCs consisting of colloidal silica dispersed into PMMA or PS have been studied. Solvent blending of PMMA with colloidal silica was performed by Carotenuto,[10] producing good dispersions. The solvent system used was methoxypropylacetate, which may have contained residual amounts of water and ethanol. The glass transition temperature of the resulting 50 wt % PNCs was 96 °C. PMMA has also been grafted onto colloidal silica by Mauger[11−13] and by Akcora.[14] Mauger's work produced good dispersions and demonstrated that the silica acted as a cross-linking site for the matrix, producing changes in the composite consistent with such a physical change. Ackora showed that combining grafted silica into the homopolymer matrix resulted in phase separation, and the resulting mechanical properties are consistent with expectations for such morphology. Etienne produced nanocomposites where the dispersion was good when PMMA was grafted onto the surface, but not good when the particles were melt-blended into the system.[15] Hub showed that the processing of the composite influenced the final properties.[16] The dispersion of the silica in the composite, processed via methyl ethyl ketone (MEK) solvent, was not ideal. Even so, they were able to demonstrate the necessity of annealing the samples

Received: July 25, 2011
Revised: September 1, 2011
Published: September 16, 2011

for 3 days to eliminate spurious effects on the glass transition temperature. Munstedt used dichloroethane as a solvent system for PMMA PNCs but was not able to achieve good dispersion.[17] The measured flow properties followed the expected behavior for filled materials. The overall trend observed was that it was necessary to have grafted particles to avoid agglomeration or to use a properly chosen solvent.

Achieving dispersion of colloidal silica in PS, a nonpolar polymer, has proven more difficult. Sen's work showed no change in chain conformation from Gaussian statistics, but the colloidal silica particles were not fully dispersed.[18] With polystyrene chains grafted onto the silica surface, Ackora showed that phase separation occurred.[19] These works both used MEK as the solvent system. Jouault et al.[20] were able to produce nanocomposites with a uniform distribution of colloidal silica aggregates but were not able to fully disperse the filler particles. The colloidal silica used in those experiments was not surface capped, so there was clearly an enthalpic mismatch between the filler and the matrix. Since long chain grafting was not successful in producing stable nanocomposites, and uncapped material is not energetically favorable for dispersion, molecular grafting of a single phenyl group onto the surface presented itself as a potential method for dispersing silica into PS.

In addition to the aforementioned specific examples relating to the materials in this study, other PNCs have been investigated for property enhancements. The fundamental question of whether polymer properties change in the presence of nanoparticles was addressed by Bogoslovov et al., who demonstrated that the addition of silica to poly(vinyl acetate) did not significantly change the properties of the polymer.[21] The nature of the bound polymer layer in systems with attractive interactions between the filler and matrix was reported by Harton et al., who used colloidal silica to demonstrate that the thickness of the bound layer of poly(2-vinylpyridine) was reduced from 4 to 1 nm upon going from a flat surface to a nanoparticle surface.[22] For electrical applications, Roy et al. measured the electrical properties of polyethylene−silica composites and demonstrated an increased resistance to electrical stress.[23] The structure of silica dispersed in poly(ethylene oxide) and poly(tetramethylhydrofuran) was studied by Hall et al.[24] PRISM theory worked remarkably well at predicting the structure of the nanocomposites. However, these studies were performed in the colloid limit, where the radius of the silica is larger than the radius of gyration of the polymer. In summary, while silica is a workhorse filler material, there do not appear to be reliable design rules enabling control of its dispersion in various polymer hosts. The current work describes how charge stabilization can be exploited to solve some of these difficulties.

For our discussion, we describe a sample with maximal interfacial area as being well-dispersed (we prefer to avoid the use of the term "random" to describe such dispersions). If the structure of the filler in a nanocomposite is consistent with the hard-sphere potential, it may be described as well-dispersed. Clustering in the structure can be interpreted as a negative departure from well-dispersed. The resulting composite will not have maximal interfacial area between filler and matrix. Alternatively, if ordering could be introduced into the solid phase, the composite would still be well-dispersed, with additionally some regularity to the spacing between particles. For experimentalists, exercising some control over this structure is useful and valuable.

Polymeric nanocomposites can be prepared from the solution state, where the particles are dispersed in solvent, and the binder (and potentially a cross-linker) is dissolved or dispersed in that same solvent, to create a formulation that may also include surfactants, antifoam agents, levelers, etc. In this type of formulation, a coating is applied to a surface, by spin-coating, application with a doctor blade or wire wound rod or directly applied to a web via a slot die. The wet coating applied to the substrate then dries, and the polymeric nanocomposite is produced. During this drying process, the thickness of the sample decreases. The nanoparticles in the formulation move and rearrange during drying. While drying, the filler particles experience forces that can be electrostatic (charge stabilized colloids), steric, and thermal (diffusive). Phase separation (particle aggregation) can occur if these forces are not managed effectively.

It is interesting to understand how particles move and rearrange during drying. Some knowledge here would aid in the control of the final structure. This paper reports our studies of drying of simple nanocomposite formulations. Herein we report on the drying of colloidal silica particles in both polystyrene (PS) and poly(methyl methacrylate) (PMMA). The silica is dispersed in *N,N*-dimethylformamide (DMF), which also serves as the polymeric solvent. We characterized the structure of the formulations using small-angle and ultra-small-angle X-ray scattering (SAXS). We report the SAXS results from the silica dispersions, from the formulated systems as a function of solvent content, and from thin films. We confirm that, in this system, the colloidal silica is charge stabilized. The formulations dry in two stages. In the first stage, the formulation simply concentrates down, retaining its charge stabilized nature. In the second stage, the charged double layer collapses, and the particles are able to diffuse more freely, resulting in cluster formation. However, for coatings, we have identified conditions under which the diffusion can be kinetically suppressed during the final stage of drying, resulting in well-dispersed nanocomposites with minimal clustering. In this manner, the charge stabilized colloidal structure can be exploited to template the structure of the final nanocomposite.

EXPERIMENTAL SECTION

The starting colloidal silica was ammonium-stabilized Ludox AS40 (Aldrich). This was transferred to DMF by adding the dispersion to DMF and then distilling off the water. This is referred to herein as unmodified silica. The silica was capped by adding phenyltrimethoxysilane (PhTMS, Aldrich) and refluxing for several hours. The capping agent enabled the silica to be dispersed into polystyrene. The capping agent was added to target 2 surface functional groups per square nanometer. The final functional group density was determined by size exclusion chromatography. When this dispersion was passed over a column, the unattached capping agents passed through the column after the capped silica. By measuring the UV absorbance of the eluent, we measured the relative amounts of attached and unattached capping agent. From this we determined that ∼70% of the capping agent was attached to the silica. In our experiments, the unattached capping agent was not removed from the dispersion. When formulated, the unattached material accounted for at most 10 vol % of the total filler loading, so that e.g. a 10 vol % loaded sample may have, at most, 1 vol % of unattached capping agent.

The dispersions were characterized by dynamic light scattering (DLS), ζ-potential, and SAXS. The DLS data were acquired with a Brookhaven BI-9000, and the ζ-potential used the PALS zeta potential

Table 1. Properties of Colloidal Silica Dispersions in DMF

particle	median diameter (nm)	polydispersity index, σ	ζ-potential (mV)	residual water content (%)
unmodified silica	28.6 ± 0.3	0.115 ± 0.019	−38 ± 6	0.42
phenyl-capped	28.7 ± 0.3	0.107 ± 0.009	−65 ± 12	0.09

analyzer. We assumed that the particle sizes were distributed in a log-normal fashion.[25,26]

Two polystyrenes were used. The first had MW = 265 kDa, with a polydispersity of 2.6 (Aldrich). The second had MW = 650 kDa, with a polydispersity of 1.1 (Pressure Chemical). The T_g of these polymers was 105 °C as measured by the inflection point of the second heat in differential scanning calorimetry (DSC). Two PMMA samples were used. The first had MW = 107 kDa, with polydispersity of 3.3 (Aldrich), with T_g = 124 °C. The second had MW = 600 kDa, with polydispersity of 3.3, with T_g = 124 °C (Aldrich). The polymers were used as received. Solutions of 10 wt % were made in DMF by allowing the solutions to roll on a mill for several weeks.

Formulations were made by simple mixing of the colloidal silica dispersion and the polymer solution on a roll mill. Formulations were cast onto either glass or Kapton substrates. The substrates were vacuum mounted to an aluminum block attached to a hot plate. The hot plate was adjusted such that the surface temperature of the substrate was 100 °C. The casting was accomplished with a doctor blade with either a 6 or 10 mil spacing. The resulting films ranged in thickness from ∼5−20 μm. The films were dried on the hot plate for ∼5 min, at which point they were dry by visual observation and then, if needed, transferred to a vacuum oven with flowing nitrogen gas for complete drying at 150 °C. Complete drying could be obtained in 72 h, as determined by thermogravimetric analysis (TGA) measurements. For the SAXS measurements, the coatings were dried only overnight (∼12−18 h) in the 150 °C oven under flowing nitrogen. For DSC measurements, the samples were dried for at least 4 days.

Freestanding films were obtained by scoring the coating into squares measuring 1 cm on each side and floated off by immersion in water. For high loadings (>30 vol %), the glass substrates were pretreated with PhTMS. A solution of 2 wt % PhTMS in isopropanol (IPA) was prepared and coated onto the glass with a #3 wire wound rod. This was air-dried, then heated in a vacuum oven with flowing nitrogen at 110 °C for 2 h, and then rinsed with IPA to remove any unattached material.

Transmission electron microscopy (TEM) samples were prepared by laminating an unfilled polymer film to the surface of a coating on Kapton polyimide film substrate in a nip laminator with rolls heated to just above the T_g of the polymer. Cross sections of nominal thickness 90 nm were prepared by ultramicrotomy of epoxy embedded laminate samples. This construction makes it possible to distinguish between the structure at the top (air) side of the coating and the bottom (Kapton) side of the coating in the TEM images. This also prevented any possible disruption to the surface of the composite that could be introduced by the liquid epoxy potting mixture infiltrating the PNC prior to cure.

Small-angle X-ray scattering (SAXS) experiments were performed using beamline 5ID-D of the Dupont−Northwestern−Dow Collaborative Access Team (DND-CAT) Synchrotron Research Center at the Advanced Photon Source, Argonne National Laboratory. As the data were collected over the course of the experiment, various beam energies (8−17 keV) and tank lengths (1−8.6 m) were used. The slit size was maintained at 0.2 × 0.3 mm^2. A flow cell was used for the scattering from the liquid dispersions to determine form factors and structure in the initial dispersions. A capillary mounted to a hot stage was used for the evaporation experiments. A plate holder was used for scattering from the thin films. Throughout this work, we assumed that the scattered intensity was the product of the form factor $P(q)$ and the structure factor $S(q)$:

$$I(q) = \Delta\rho^2 V \phi S(q) P(q) \quad (1)$$

The proportionality constants are the electron density difference between the polymer and the silica $\Delta\rho$, the average volume of an individual scatterer V, and the loading fraction ϕ. $S(q)$ was extracted by dividing $I(q)$ by $P(q)$. This analysis is only valid if the polydispersity is low, and we assumed that the measured polydispersity index of 0.11 was an acceptably low value (see Table 1). The processing was done within Excel so that the Solver routine could be used. SAXS from an unfilled polymer film was used as the baseline scattering curve. This curve was subtracted from the data. The baseline was multiplied by a scaling factor optimized to make the slope of $I(q)q^4$ = 0 in the range 0.1 < q < 0.2 Å^{-1}. Long tank and short tank data were then merged by minimizing the sum of the squares of the $I(q)$ values in the overlap regions of the data sets by multiplicative amplitude adjustments on the USAXS data, along with a scaled baseline subtraction (again, this baseline was taken from the appropriate unfilled polymer film). USAXS data were linearly interpolated in the overlap region to q values that exactly matched the SAXS data to enable the calculation of the differences.

The form factor $P(q)$ was initially assumed to be equal to the shape of the $I(q)$ curve at a volume fraction of 0.1 vol % for the nanoparticle dispersion in solvent. The $P(q)$ curves were baseline corrected from suitable blanks, again with the goal that the slope of $P(q)q^4$ = 0 in the range 0.1 < q < 0.2 Å^{-1}. We discovered that, even at this low loading, there was still some residual structure in the scattered intensity for q < 0.005 Å^{-1}. To correct for this, we used the extracted parameters for the colloid size and polydispersity (see Table 1) and extrapolated the values for the scattered intensity to the low q range. This extrapolated curve was then spliced onto the experimental curve to eliminate the structure in the scattering from the 0.1 vol % loading scattered intensity. This spliced $P(q)$ was then used when eq 1 was applied to the data.

Equation 1 was applied to the merged data sets by dividing the scattered intensity by $P(q)$. After division, a multiplicative factor was applied to make the average $S(q)$ = 1 for that same q range. This multiplicative factor was generally, but not exactly, equal to the ratio of the volume loading of the sample relative to 0.1 vol % (the form factor volume loading). This procedure was followed for the liquid dispersions and the thin films. For the *in situ* drying experiment in the capillary, only USAXS data were collected (tank length 8.7 m, beam energy 9 keV). To measure that scattering, an aliquot of formulation was placed into an open glass capillary, which was mounted into a hot stage in the X-ray beamline. A canula supplying dry nitrogen gas was inserted into the open end of the capillary to expedite solvent removal. After the sample was mounted, the hot stage was heated to 150 °C. As the sample heated and dried, X-ray scattering was measured in 10 s intervals, with the beam passing through the bottom, closed end of the capillary. The form factor was divided out with no baseline adjustments to the scattered intensity, and the resulting structure factor was set equal to unity at q = 0.05 Å^{-1} for the scaling.

Differential scanning calorimetry (DSC) was performed on a TA Instruments Q1000. The sample was heated from 0 to 160 °C at 10 K/min, held at 160 °C for 10 min, cooled at 10 K/min to 0 °C, and then reheated to 160 °C at 10 K/min for the second heating.

RESULTS AND DISCUSSION

Characterization of Colloidal Structure in Solvent. The size distributions of the particles for the colloidal silica dispersions in

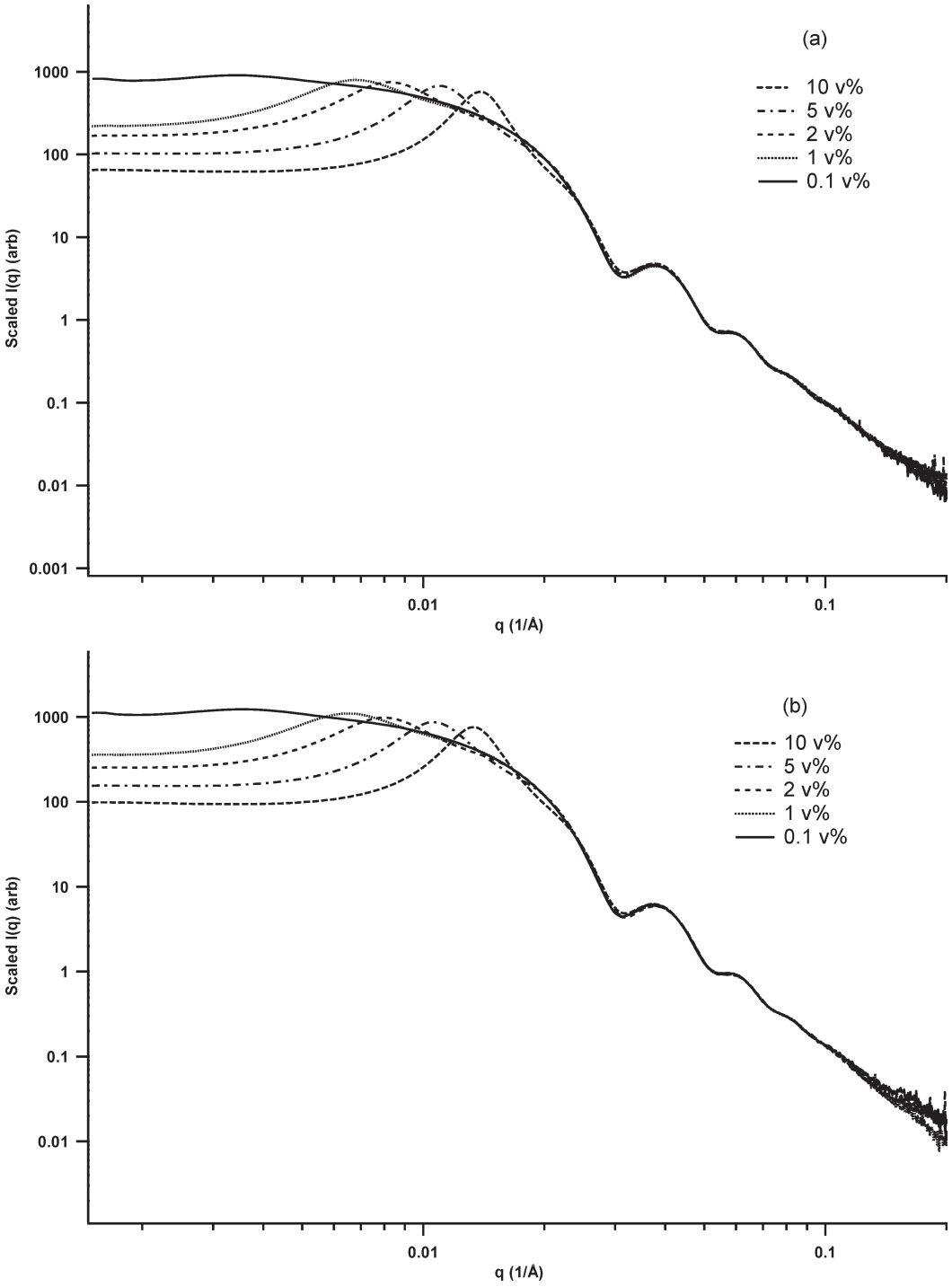

Figure 1. Scaled, combined small-angle and ultrasmall-angle X-ray scattering from (a) unmodified colloidal silica and (b) phenyl-capped colloidal silica dispersed in DMF as a function of volume percent.

DMF were characterized by SAXS. Scattering from 0.1 vol % dispersions was taken as representative of the form factor, $P(q)$. These were fit to a log-normal distribution using SAXSFit software.[27] Table 1 reports the median particle size and the polydispersity index.

DLS was also used to characterize the particle size, and those results agreed with the SAXS results. As an example, for a 0.1 wt % sample of phenyl-capped silica dispersed in DMF, the effective diameter was 32.2 ± 0.3 nm, with a polydispersity of 0.158 ± 0.007. We analyzed this result assuming that the particle sizes were distributed lognormally.[28] In this case, the relationship between the shape parameter of the log-normal distribution and the polydispersity as measured by DLS is

$$\frac{\langle(\delta D)^2\rangle_z}{\langle D\rangle_z^{\,2}} = \exp(\sigma^2) - 1 \qquad (2)$$

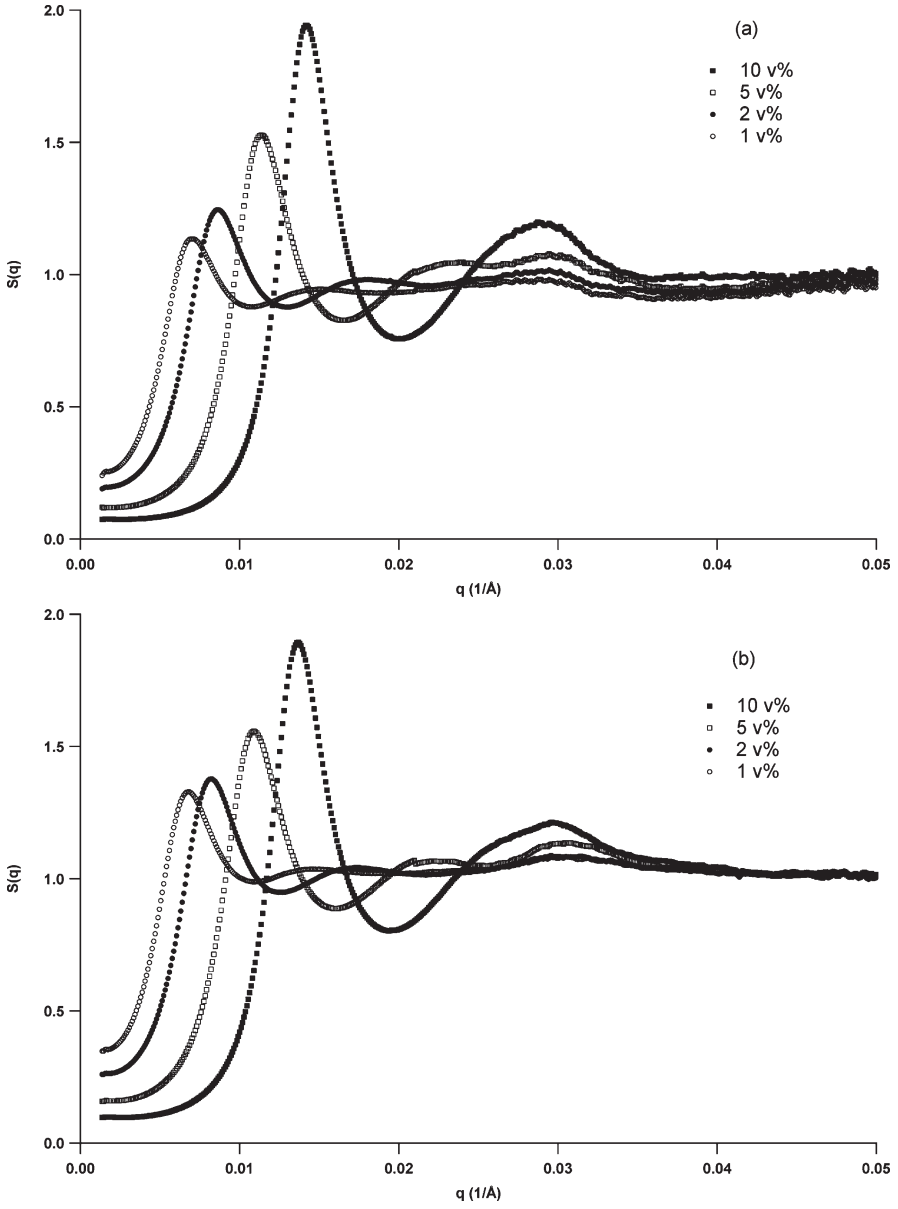

Figure 2. $S(q)$ for (a) unmodified colloidal silica and (b) phenyl-capped colloidal silica dispersed in DMF as a function of volume percent.

Given a polydispersity of 0.158, we derive that $\sigma^2 = 0.0157$. The median particle size is given through the relationship

$$\langle a \rangle_z = \exp\left(\mu + \frac{11\sigma^2}{2}\right) \tag{3}$$

From this, we determined that $\mu = 3.38$, and the median particle diameter is $e^{\mu} = 29.5 \pm 0.3$ nm, acceptably close to the SAXS value of 28.7 ± 0.3 nm. A possible explanation for the slight discrepancy is the fact that DLS measures the hydrodynamic radius of the particles, while SAXS measures the radius at which the density is discontinuous.

The surface charge was characterized by ζ-potential, which was measured on dispersions of 0.01, 0.1, 1, 2, 5, and 10 vol %. No systematic trend in ζ-potential was observed as a function of volume fraction, so the reported numbers are for the average value, along with the standard deviation. Since the particles have a large screening length (detailed below), the electrophoretic mobility was converted to the ζ-potential using the Huckel approximation for Henry's function. Henry's function equals unity under the Huckel approximation and 1.5 under the Smoluchowski approximation (small screening length).[26] The results of these analyses are summarized in Table 1. Also included in Table 1 is the residual water content for the dispersions.

To summarize, the particles are ∼30 nm in diameter and reasonably monodisperse. The ζ-potential measurements, while scattered, do support the conclusion that the dispersions are charge stabilized, regardless of surface treatment. We cannot determine if the ionized proton from the surface silanol group is stabilized exclusively by the DMF solvent or if residual water assists in the complexation.

To further understand the nature of the charge stabilized dispersions, SAXS was performed at 0.1, 1, 2, 5, and 10 vol % silica loading. Figure 1 displays the scattered intensity as a

dx.doi.org/10.1021/ma201714u |*Macromolecules* 2011, 44, 8301–8313

function of wavevector for the unmodified and phenyl-capped dispersions as a function of volume loading, appropriately scaled to overlap in the Porod region. Our analysis in this section roughly follows the work of Qiu et al.[29] The structure factors for the two dispersions are shown in Figure 2. There are only minor differences between the two dispersions.

The structure factor was analyzed with both the effective hard sphere (EHS) model and the Hayter−Penfold mean spherical approximation (HPMSA) model.[30] The EHS model assumes that there is a core hard sphere, with diameter d_{HS}, dressed with a charged shell, of thickness δ, such that the particle has an effective diameter, d_{eff}. A schematic depicting the relevant geometrical parameters is shown in Figure 3. Fitting to $S(q)$ provides d_{eff} and the effective volume loading ϕ_{eff}. Fits to the EHS model were constrained to the first peak in the data. The model did not fit the second or third peaks of the data, presumably due to polydispersity effects. The shell thickness is given by

$$\delta = \frac{d_{eff} - d_{HS}}{2} \tag{4}$$

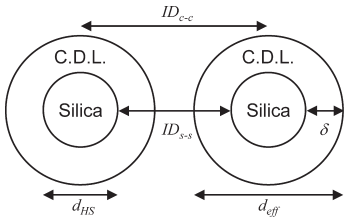

Figure 3. Schematic representation of two charged colloid particles denoting the meaning of the geometric parameters. $ID_{c\text{-}c}$ is center-to-center interparticle distance. $ID_{s\text{-}s}$ is surface-to-surface interparticle distance. d_{HS} is the hard-sphere diameter. d_{eff} is the effective diameter of the charged colloid. δ is the shell thickness. CDL stands for charged double layer.

It is worthwhile to compare 2δ to the surface-to-surface interparticle separation, $ID_{s\text{-}s}$, given by

$$ID_{s-s} = d_{HS}\left(\left[\frac{\phi_{max}}{\phi}\right]^{1/3} - 1\right) \tag{5}$$

In this relation, ϕ_{max} is the maximum packing fraction of spheres, which was approximated here as $2/\pi = 0.637$ for random dense packing, but can be as large as $\sqrt{2}\pi/6 = 0.74$ for an fcc lattice.[31] This comparison, displayed in Figure 4, provides insight into how crowded the dispersion was. We see that the shell thickness varied appreciably with particle concentration, decreasing at higher concentrations. The dressed particles are almost close packed at 10 vol %, where $2\delta/ID_{s\text{-}s} \sim 0.75$. This is an indication that the charged double layers may be overlapping between adjacent particles. Thus, the particles are interacting relatively strongly with one another. Compared to Qiu,[29] who observed that $\delta \sim 20-40$ Å for aqueous colloids, we observe $\delta \sim 100-300$ Å.

The Hayter−Penfold mean spherical approximation (HPMSA) model predicts the structure of charged colloids interacting via the screened Coulomb potential,[30] and we applied it to the data to gain further insight into the structure of the dispersion. There are ostensibly six parameters in this model. Two of them, the dielectric constant of DMF ($\varepsilon = 37$) and the temperature (298 K), were known. A third, the volume loading ϕ, was known precisely from the preparation of the formulations. We considered the ionic concentration, the fourth parameter, as a factor that was present in the parent dispersion and inherited by the daughter preparations. Since the various concentrations were made as dilutions from the parent stock solution, there was a known relationship between that salt concentration and that of the dilutions. We assumed varying values for the parent salt concentration and fit the remaining two parameters, the hard-sphere diameter and the surface charge, creating a response curve for the system. Fits were performed within IGOR. The parent salt

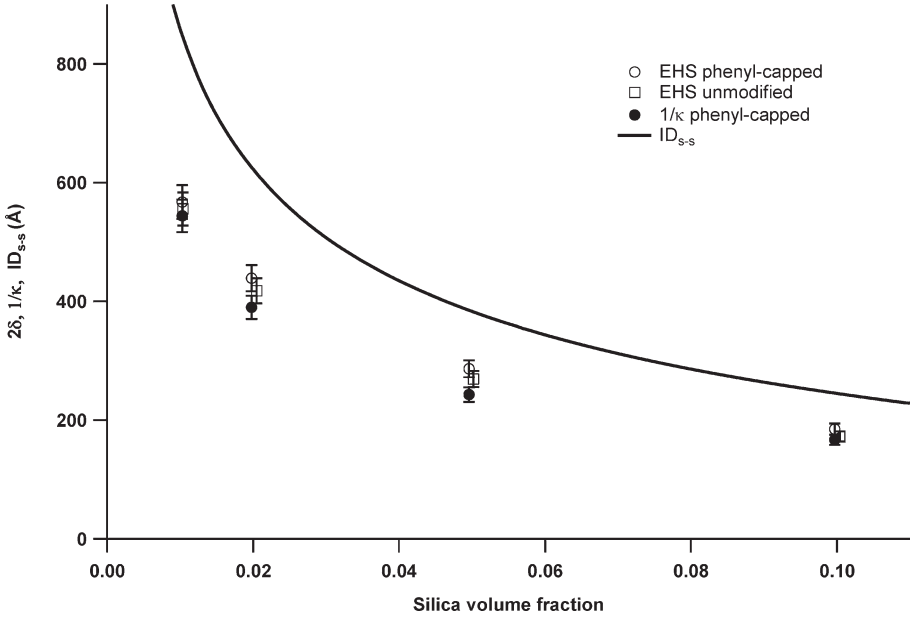

Figure 4. Volume fraction dependence of model parameters: interparticle surface-to-surface distance ($ID_{s\text{-}s}$, solid line); two times the shell thickness (open symbols); Debye decay length (closed symbol).

Table 2. HPMSA Model Parameters

volume loading (nominal)	1 vol %	2 vol %	5 vol %	10 vol %
diameter d_{HPY} (Å)	289	288	288	287
charge (e^-/particle)	37.3	43.9	67.6	94.4
volume fraction (exptl)	0.0103	0.0198	0.0496	0.0997
monovalent salt conc (M)	1.47×10^{-5}	2.86×10^{-5}	7.38×10^{-5}	1.56×10^{-4}
Debye screening length, $1/\kappa$ (Å)	544	390	243	167
$\kappa d_{HPY}/2 = \kappa a$	0.27	0.37	0.59	0.86
surface potential ψ_0 (mV)	46	52	72	86
dimensionless Yukawa constant U_0/kT	15.4	19.5	37.5	53.7

concentration of 2×10^{-4} M was chosen as the most likely value for this parameter because this choice resulted in the minimization of the surface charge on the silica at all volume loadings and hence the chemical potential of the system. At higher or lower salt concentrations, the model's fits predicted a larger surface charge. This should be interpreted as an effective salt concentration, such that it models the screening of the Coulomb potential. It includes the effect of all ionic species present in the system, both the ions that dissociated from the colloidal silica, and any other salts present in the system. In addition, this choice of the salt concentration resulted in hard-sphere diameters that closely agreed with those obtained from the form factors $P(q)$. Since the structures for the dispersions were practically identical, we performed the HPMSA fits to only the phenyl-capped colloidal silica. The results are collected in Table 2. The fitting parameters are displayed in the top section, and the values derived from them are in the bottom section. We observed that the fitted hard-sphere diameter matched, within error, that from $P(q)$. The surface charge was seen to increase with volume concentration. The surface potential was close to that measured by ζ-potential. Figure 4 displays the resulting values for the Debye screening length; it is roughly equal to twice the shell thickness deduced from EHS fitting. The product $\kappa a < 1$ for all samples, justifying the Huckel approximation to Henry's function. The HPMSA fits implied that the ionic strength of the dispersion was low. This is understandable because ionic species and inorganic salts are generally not very soluble in DMF, and the initial dispersion was ammonium stabilized, not sodium stabilized. When the water is boiled off from the DMF, the ammonia will also be removed, since it has a vapor pressure ∼60× that of water at 100 °C.[32] In this situation, the Coulomb potential is weakly screened. From these analyses, we concluded that the spatial extent of the charged double layer was large in these samples, so that the particles interacted with each other quite strongly, even at 1 vol % concentration. Given the large Debye screening lengths, which indicate strong spatial overlap between the charged double layers on adjacent particles, it is not clear if the HPMSA potential is an appropriate representation of the interaction energy in this system.

The structure was independent of surface treatment, demonstrating further that these colloids were charge stabilized, not sterically stabilized. From the HPMSA analysis, we note that there were fewer than 100 charges per silica particle. Assuming that there were 4 silanols per nm^2 of silica surface area, and given the 28.7 nm diameter, we calculated that <1% of the silanols were ionized. Stabilizing the silica required relatively few ionized silanol groups, and it was possible to chemically cap the surface with phenyl groups and still have enough free silanols to create charge stabilized dispersions.

Drying of Formulations. In the second stage of the experimentation, we examined how the SAXS pattern changed as solvent was evaporated from a formulation. Formulations were made that contained 10 vol % total solids, where the solids are partitioned between colloidal silica and polymer. The ratio of silica to polymer determined the final volume percent of silica in the composite. Four systems were examined: the unmodified colloidal silica dispersed in high and low molecular weight PMMA and the phenyl-capped colloidal silica dispersed in high and low molecular weight PS. Each of these was done at a variety of loadings such that the volume fraction ϕ of silica in the dried formulation was between 1 and 50 vol %.

The result of a representative drying experiment is shown in Figure 5. This figure shows the extracted $S(q)$ for a 30 vol % phenyl-capped colloidal silica: 265K MW PS formulation in DMF. (30 vol % refers to the volume fraction of colloidal silica in the final, dried sample. Thus, this formulation was initially 3 vol % silica, 7 vol % PS, and 90 vol % DMF). At time zero, $S(q)$ matched the scattering for the charged colloid in DMF without polymer. This scattering was dominated by the feature at $q \sim 0.01$ Å^{-1}. We did not observe phase separation in the initial formulation. As the sample began to dry, the peak in $S(q)$ gradually shifted to higher q. From this we concluded that the formulation maintained its charged colloid structure but concentrated to higher percent solids. When the EHS model was fit to this peak, we determined that the concentration of colloidal silica approximately doubled prior to the peak's decrease in intensity. This indicated that about half the solvent had evaporated when the peak started to decay. Concentration characterizes this first stage of drying. In this stage, the charged colloidal structure was maintained in the formulation. This stage lasted for the first ∼1500 s in this experiment.

Phase separation in this stage, by either depletion flocculation or some other cause, was suppressed by two mechanisms. First, the charged nature of the colloid provided a repulsive force that prevented agglomeration. Second, the formulation contained a large amount of polymer, such that it was in the semidilute regime. The polymer in solution was entangled with other chains. The simple picture of a polymer chain diffusing out of the depletion zone is not applicable here. The polymer formed an entangled mesh which contracted as the solvent evaporated.

After ∼1500 s, a dramatic change in the scattering occurred. The charged colloid peak disappeared and was replaced by scattering at $q \sim 0.027$ Å^{-1} and at $q < 0.01$ Å^{-1}. As the solvent evaporated, the chemical potential of the polymer plus solvent environment shifted such that solvation of protons was no longer thermodynamically favored. In other words, the evaporation of

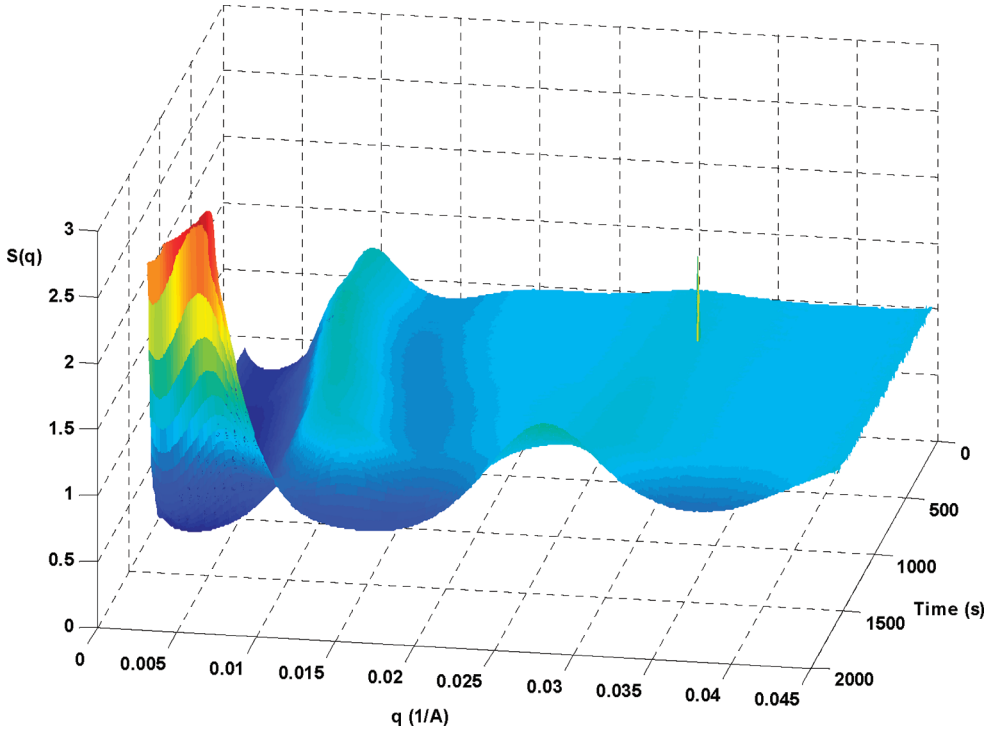

Figure 5. Evolution of $S(q)$ with time as a function of drying for the 30 vol % phenyl-capped silica/265K MW PS/DMF formulation.

the DMF reduces its concentration and shifts the equilibrium for proton dissociation toward the neutralized colloid. This caused the charged double layer to collapse, and protons that were solvated by the DMF reverted back onto the surface of the silica, neutralizing it. This reduced the surface charge of the colloid, which in turn allowed phase separation, by either depletion flocculation or some other mechanism, to occur.

As flocculation (phase separation) occurred, particles came into contact with one another, characterized by a scattering peak at $q \sim 0.027$ Å^{-1}, regardless of the final silica volume loading. At this wavevector, $qd_{HS} = 7.7$ for $d_{HS} = 287$ Å^{-1}. When one considers the model of the monodisperse, hard-sphere structure factor, a volume fraction of $\phi \sim 0.65$ creates a peak in $S(qd_{HS})$ occurring at $qd_{HS} \sim 7.7$. Thus, we interpret the peak at $q \sim 0.027$ Å^{-1} as an indication of a phase consisting of particles packed at a density near the random dense packing limiting volume fraction. As the particles agglomerated into larger clusters, scattering at low q increased. In cases where an identifiable peak occurs at low q, we can associate the size of the cluster with $2\pi/q$. In Figure 5, we observed a peak in the scattering corresponding to a cluster size of ~200 nm.

We have not yet been able to measure the surface charge as a function of solvent composition. However, we can safely assume that when the formulation is fully dry, very few, if any, protons will be solvated by the PS matrix. As the polarity of the PS/DMF system shifted to being less polar as the DMF evaporated, the ability of the system to solvate protons decreased. Thus, neutralization of the colloid must have occurred. To what extent it occurred relative to the aggregation phenomenon still needs to be investigated. This second stage of the process we refer to as collapse of the charged double layer (neutralization) and drying.

The behavior shown for this formulation was qualitatively replicated by all the formulations regardless of silica loading or matrix polarity. The PMMA samples showed the same features. This general scheme of concentration, followed by collapse of the charged double layer (neutralization) and drying, is common to all the systems studied here.

Characterization of Thin Films. In the third stage of experimentation, we prepared freestanding PNC films and measured the structure of the colloidal silica filler using SAXS. Our goal was to prepare films for diffusion studies,[33] where it was necessary to produce films with uniform particle density at a surface, with no clustering. This was achieved by casting the formulation onto a substrate maintained at an elevated temperature. When the substrate's temperature was room temperature, significant clustering was observed at the PNC−glass interface, although the particles were well-dispersed in the middle of the coating. As the substrate's temperature was raised, the clustering at the buried interface decreased. A balance between uniformity and practicality was found with substrate temperatures ~100 °C for DMF formulations. At these temperatures, the DMF dries relatively quickly, and the reduced setup time influenced the quality of the dispersion. Residual structure at the coating−air interface could not be avoided but was localized to a region ~100 nm in thickness. For the published diffusion studies,[33] the films were floated off the glass by immersion in water, and the deuterated polymer was coupled to the well-dispersed, buried interface side of the sample.

SAXS experiments were carried out on freestanding PNC films and removed from their glass substrates by immersing the plate in water and allowing the films to release from the effect of water surface tension wicking into the buried interface. For the higher volume loadings, a single film ~10 μm thick provided sufficient signal. For lower volume loadings, several films were stacked together to provide good signal-to-noise. The scattered intensity was divided by the form factors determined from the dispersions to extract $S(q)$. Figure 6 shows $S(q)$ for the four PNCs as a function of volume loading. Figure 7 shows TEM images for the

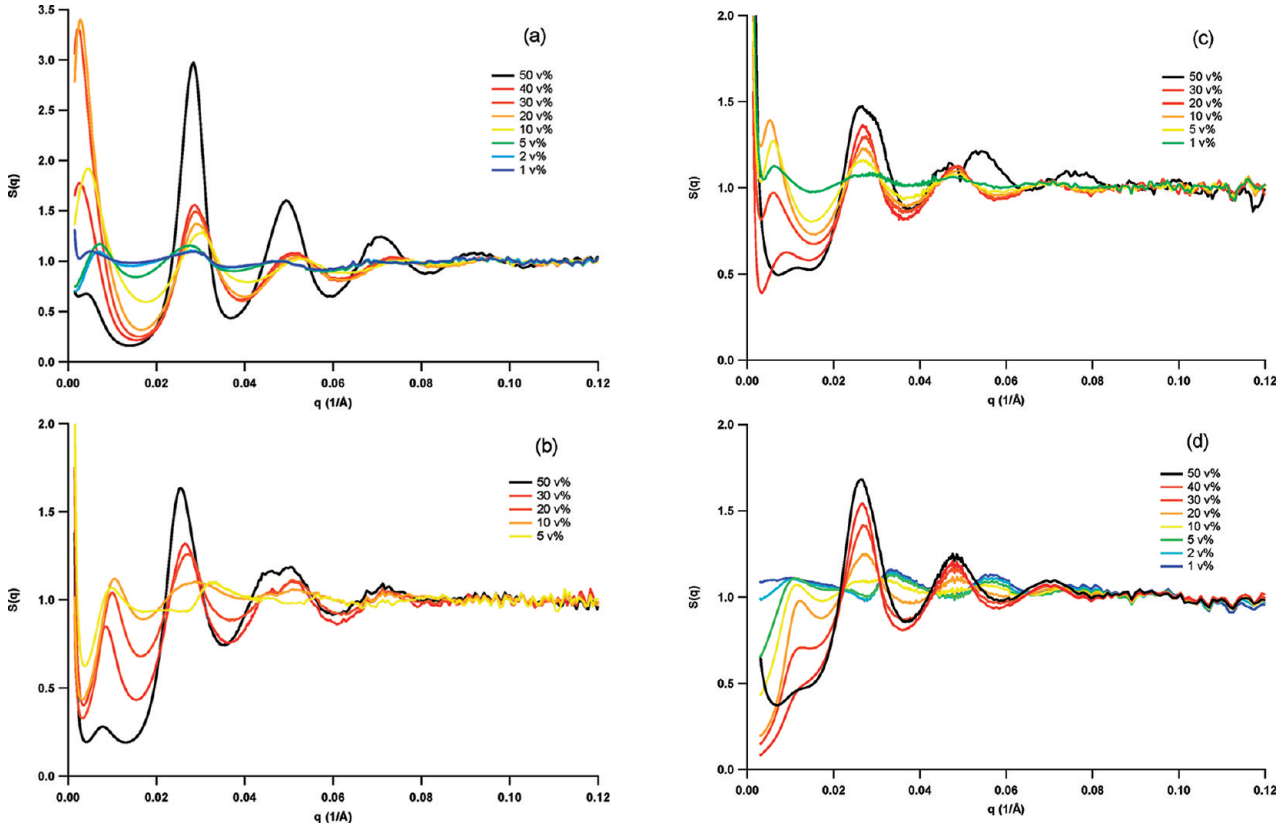

Figure 6. $S(q)$ for the four composites: phenyl-capped silica in 265K PS (a); phenyl-capped silica in 650K PS (b); unmodified silica in 107K PMMA (c); unmodified silica in 600K PMMA (d).

10 vol % PNCs, respectively. The TEM sections came from the same exact coating, albeit from an adjacent location, as was examined by SAXS. This enables one to compare the spatial images with their q-space representations. We chose 10 vol % for representative TEM images because the microtome slices were ~100 nm in thickness. Samples with silica loadings greater than 10 vol % are hard to visually analyze because of overlap between particles that were spatially stacked over one another, even if they were not in contact.

The low-MW PS composites clearly showed clustering behavior (Figure 6a), similar to the result of the capillary drying experiment. The 1 vol % loading showed little structure, due to the large average interparticle spacing. The 2 and 5 vol % loadings were beginning to show clustering, and this increased as the loading increased. The level of clustering in the 10 vol % sample is visualized in the accompanying TEM image. Clearly particles were contacting one another, but the particles were uniformly distributed. There were no large clumps of particles separated by unfilled matrix. The hard sphere peak occurs at $q \sim 0.0288$ Å^{-1} ($qd_{HS} = 8.27$), indicative of a tightly packed condensed phase. The magnitude of this peak increased with loading, indicating that the population in this phase increased. For reference, for a monodisperse hard sphere system at $\phi = 0.74$, the peak in $S(qd_{HS})$ would occur at $qd_{HS} = 8.1$. It is plausible that polydispersity could make the observed peak occur at a higher value than the monodisperse model because particles could theoretically pack to higher density in a polydisperse system.

The high-MW PS sample was qualitatively and quantitatively different (Figure 6b). The TEM image (Figure 7b) showed a more uniform dispersion. While there were still particles in contact with one another, the overall distribution was much more homogeneous. This was revealed in $S(q)$, also. The hard-sphere peak occurred at $q \sim 0.0257$ Å^{-1}, corresponding to a monodisperse hard sphere volume of $\phi = 0.59$—a less dense phase than for the low-MW analogue. The magnitude of the low-q scattering was reduced when compared with the low MW matrix, and there was a clear peak in the low-q scattering for all volume loadings. If we assume that the peak in the low-q scattering corresponds to a cluster size, we conclude that the cluster diameter was 560 Å (roughly two particle diameters) at low volume loadings and increased to 760 Å (roughly three particle diameters) at 50 vol %. For the low- MW PS case, the slight peak at low q would correspond to clusters of ~1100 Å. These cluster sizes are roughly in agreement with what one could surmise from the TEM images.

The charged colloid structure in the formulation acts as the initial condition for diffusive motion after collapse of the charged double layer. As the DMF evaporated, and the charged double layer collapsed, the colloidal particles diffused and, following Stokes relation, that diffusion constant was inversely proportional to the viscosity of the medium. With an increase in MW of ~2.5×, the solution viscosity increased by ~10×, significantly slowing diffusive motion. This inhibited the formation of large clusters. During annealing, there presumably was additional diffusion of the colloid, but the matrix viscosity was high, so this diffusive motion was quite slow. In a sense, the charged colloid structure templated the structure of the dried composite, enabled by the high viscosity of the matrix during the drying process.

The PMMA system showed behavior similar to the PS system. For the low-MW PMMA matrix (Figure 6c), the

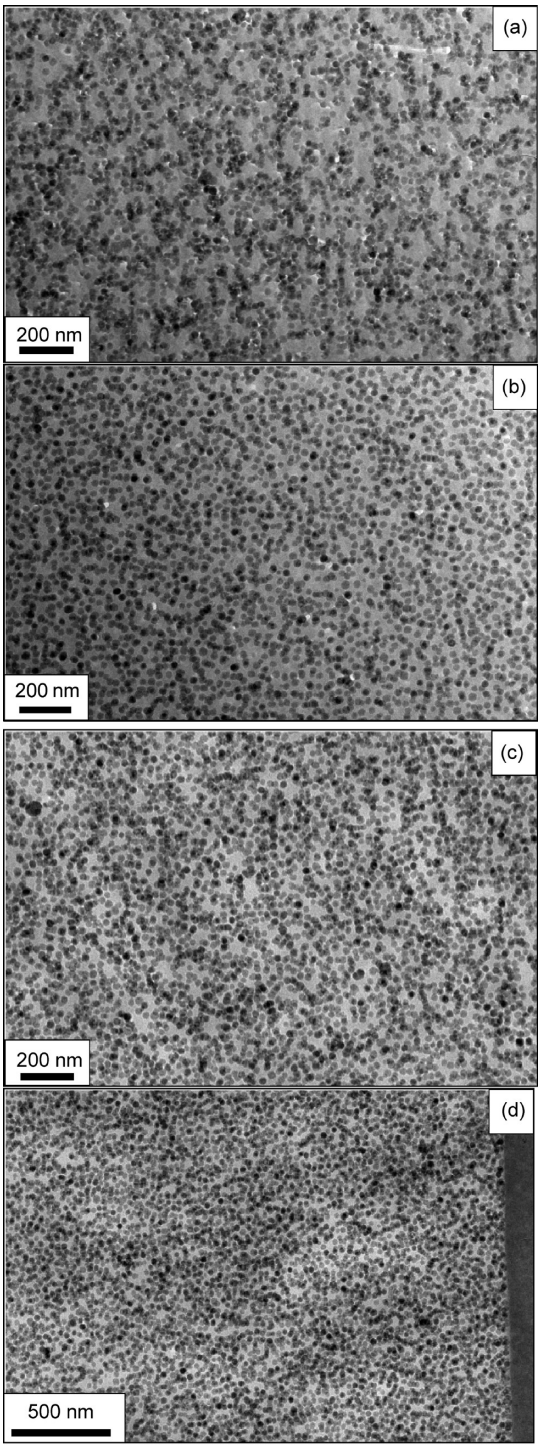

Figure 7. TEM images of the four composites at 10 vol % loading: phenyl-capped silica in 265K PS (a); phenyl-capped silica in 650K PS (b); unmodified silica in 107K PMMA (c); unmodified silica in 600K PMMA (d).

scattering was similar to that from the dried capillary experiment. Clustering was observed. The TEM indicated that this clustering was not severe in the sense that there were not any large clusters separated by unfilled matrix. The hard sphere peak was at qd_{HS} = 7.89, corresponding to a monodisperse hard-sphere volume fraction of ϕ = 0.70. For the high-MW PMMA matrix (Figure 6d), there was an absence of rising scattering at low q, and again we observed a peak in the scattering that could be interpreted as arising from clusters of roughly two particle diameters in size. In contrast to the PS case, however, the hard-sphere peak did not shift appreciably with increasing PMMA MW.

The same explanation holds for this matrix. The higher molecular weight of the PMMA increased the viscosity of the medium during drying and limited the distance over which the particles could diffuse before being immobilized within the dry coating. The TEM image of the high-MW PMMA sample displayed a more uniform appearance, too. The image (Figure 7d) also shows the edge of the film, visually demonstrating uniform particle loading at the buried interface. It is interesting to note in the $S(q)$ of this sample that the peak corresponding to particle−particle contact is absent for the 10 vol % sample but is present in the 20 vol % sample. This could be related to the 15 vol % threshold for percolation of impenetrable spheres in three dimensions. With enough charged colloid ordering, it is possible that very few particles would be in contact at 10 vol %, while very regular ordering would be necessary to suppress particle−particle contact at 20 vol % loading.

Taken together, these results demonstrate that charged colloids can be transformed into well-dispersed PNCs with minimal clustering. To accomplish this goal, it was necessary to increase the matrix viscosity during drying and to dry the sample relatively quickly. The phase transition from uniform to clusters occurred on a time scale that was influenced by the diffusion coefficient of the particles. When that diffusion coefficient was small, the phase transition could be arrested. The resulting small cluster sizes produced composites with high interfacial area.

There is a large literature on the phase transitions of polymer−colloid mixtures.[6,34−41] Some describe systems in the colloid limit,[36] where the colloid is much larger than the radius of gyration (R_g) of the polymer chain, while some are applicable in the protein limit, where the colloid is much smaller than the R_g of the polymer chain.[35] In addition, free volume theories[36] address situations where the polymer concentration is below the overlap limit, which also does not apply here. PRISM theory[37−41] perhaps has advanced the furthest but still does not capture the physics in this system. For instance, the peaks in $S(q)$ for the 20 vol % unmodified silica in 600K MW PMMA are at qd = 3.6 and 7.8. PRISM theory predicts a single peak at $5 < qd < 6$. This can be explained by recognizing that the templating produced by the charged colloid structure creates a starting configuration that is not probable, whereas PRISM calculates structure for an equilibrium configuration. Our system underwent a phase transition due to ultimately attractive forces between the particles, whereas the calculations were for a hard-sphere interparticle potential.

Understanding the structural development in this system relies on a model for the dynamics of the nanoparticles, the details of which are currently beyond the scope of this work. Qualitatively, however, we can posit a description of the process of composite formation. After the initial casting, the colloidal silica particles are structured in accord with an effective hard-sphere potential, and they remain so as long as they are charged. They are diffusing, but within a potential well created by the charge repulsion from other particles. After they are neutralized, the potential no longer acts like a cage, and they diffuse more freely. The initial condition for this diffusion problem is not that of a hard-sphere liquid with

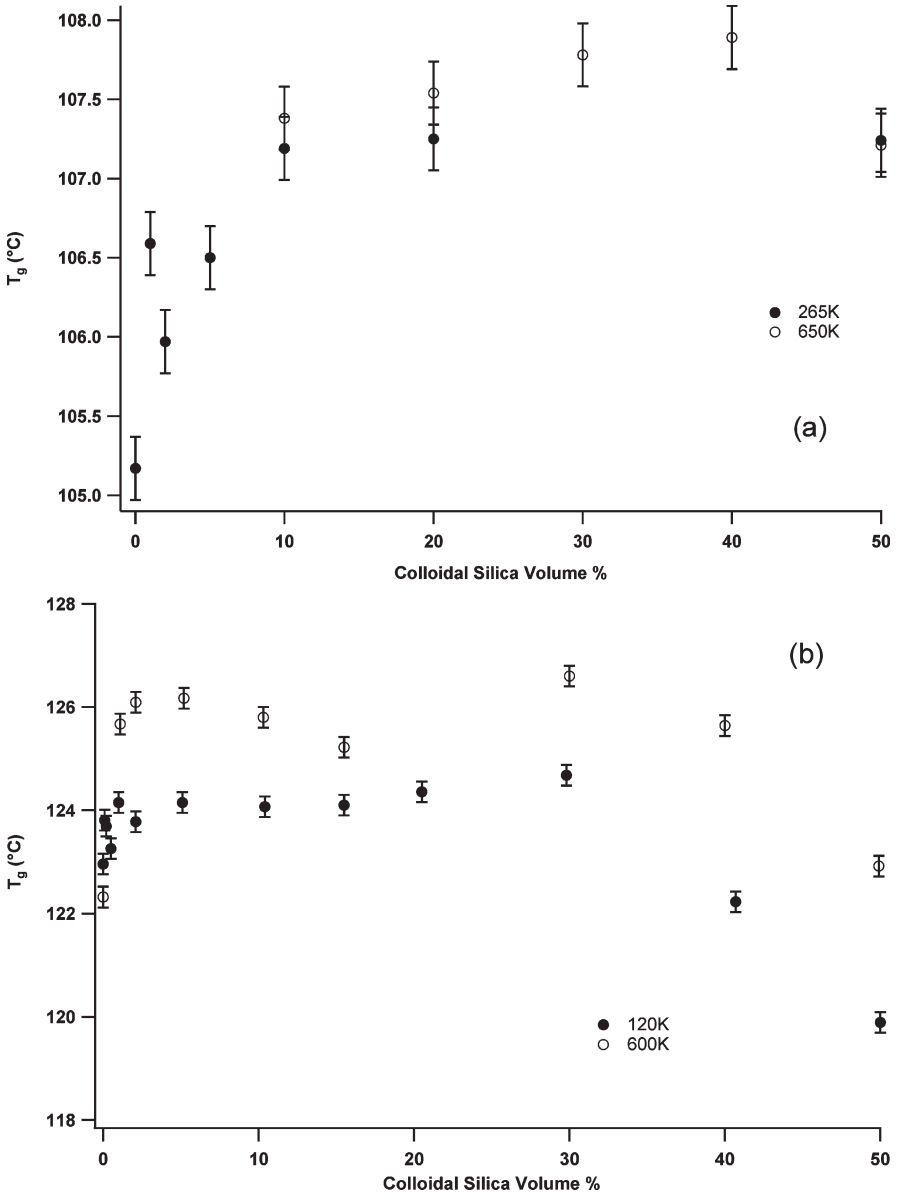

Figure 8. Glass transition temperatures for (a) PS and (b) PMMA nanocomposites.

particles of 28 nm in diameter—the remnant of the effective hard-sphere potential makes it more ordered than that. From the TEM evidence, there are clearly short-range attractive forces between the particles. The most probable process is diffusion limited aggregation starting from a relatively ordered initial configuration. The extent to which aggregation occurs is controlled by the viscosity of the medium, which depends, in part, on the molecular weight of the polymer matrix. In the early stages of aggregation, doublets form. These doublets, and other small clusters, are accounted for by the peaks in the SAXS data at $q \sim 0.01$ Å^{-1} for the high-MW matrices and are also seen in the corresponding TEM micrographs. As the aggregates increase in size, the peak in the SAXS data shifts to lower q, signaling larger clusters, as observed in the low-MW matrices. Again, this interpretation is supported by the TEM images. In this work, good dispersion is achieved when the clustering process was arrested because of high matrix viscosity produced by the rapidly drying coatings.

It is recognized that when these samples are annealed above T_g, particle diffusion will still occur. We have performed annealing experiments on the phenyl-capped silica in low-MW PS. After 1 week at 150 °C, agglomeration can be ascertained from TEM images, but only slightly; not to the extent seen by other researchers for polymer chain grafted particles.[14,19] We are in the process of quantifying this behavior with SAXS.

Glass Transition. Many researchers have been concerned with potential changes in the mechanical properties of PNCs. One such property, heat deflection temperature (HDT), is important for structural applications. The HDT is correlated with the glass transition temperature, T_g, of the base resin. For these reasons, we were interested in measuring T_g of our PNCs. In summary, we found no large change in T_g for any of the composites prepared for this study as measured by DSC. Also, the change in heat capacity associated with the glass transition, Δc_p, followed a simple rule of mixtures. There was no evidence to support the

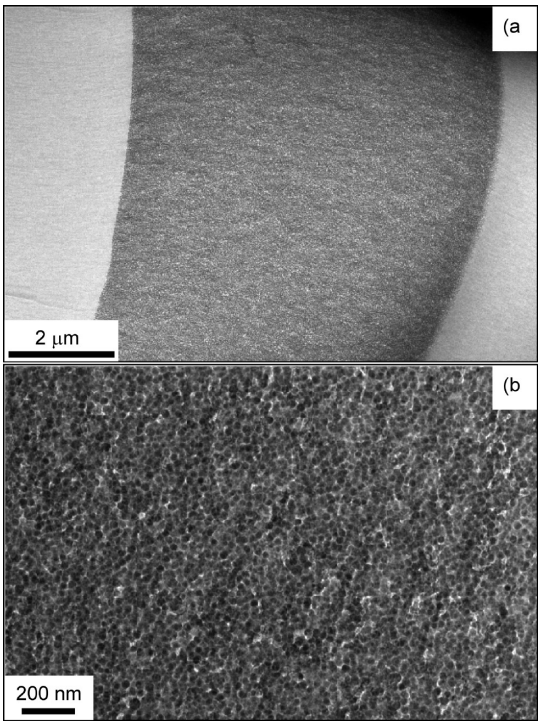

Figure 9. TEM of 50 vol % phenyl-capped colloidal silica in 650K MW PS matrix: (a) 18.2K magnification; (b) 95K magnification.

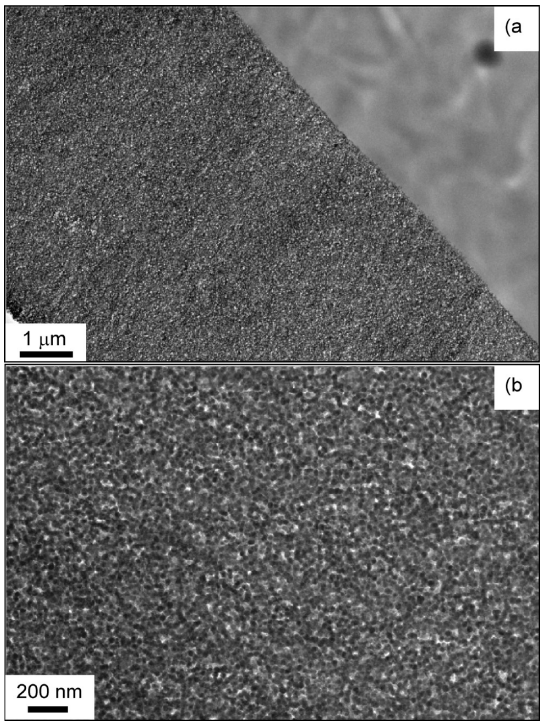

Figure 10. TEM of 50 vol % unmodified colloidal silica in 600K MW PMMA matrix: (a) 18.2K magnification; (b) 73K magnification.

existence of a polymer interphase or a rigid amorphous fraction in these composites.

The DSC data are presented in Figures 8 and 9. Figure 8a shows the T_g, as assigned to the inflection point of the DSC curve, for the polystyrene composites. There was an increase of 2 °C as the loading was increased to 10 vol %, but no additional increase after that. A TEM image of a 50 vol % composite is shown in Figure 9. The low-magnification image demonstrates good distribution of the particles, while the high-magnification image demonstrates the good dispersion.

In Figure 8b, we show the measured T_g from the PMMA composites as a function of volume loading. For the 120K matrix, the T_g for the 1 vol % composite rose ~1 °C compared to the unfilled polymer and was relatively constant for filler loadings up to 30 vol %. At higher loadings, there was a noticeable, but small, decrease in T_g, reaching ~4 °C at 50 vol %. The 600K matrix showed similar behavior. The unfilled material had a T_g = 122 °C, which increased to 126 °C at 1 vol % loading, remained constant up to 30 vol %, and then decreased ~4 °C from that level at 50 vol %. Low- and high-magnification images of the 50 vol % samples are shown in Figure 10 to depict the dispersion quality and demonstrate that the silica was not aggregated. These images enable one to visualize the extent of polymer confinement inherent in these systems.

Efforts have been made to show the analogy between PNCs and polymer thin films with regard to T_g shifts.[42] For the work presented here, it is desirable to extract an average cavity volume for the polymer phase in the highly loaded composites. To accomplish this, we apply the results of scaled particle theory (SPT),[43−45] which calculated that, at high loading, the average cavity volume is

$$\langle v \rangle = \left[\frac{d_{HS}}{pV/nkT - 1} \right]^3 \qquad (6)$$

At 50 vol % loading, the simulation predicts that the denominator equals 12.9,[45] so the average cavity volume is equivalent to a sphere with an effective diameter of 2.7 nm. From eq 5, we calculate that $ID_{s\text{-}s}$ = 2.4 nm for 50 vol % ($\phi_{max} = 2/\pi$), or $ID_{s\text{-}s}$ = 4.0 nm (ϕ_{max} = 0.74), so this may be used as a rough surrogate for the cavity dimension. Insofar as PNCs can be considered an analogous system to polymer thin films, we conclude that there is only a small shift in T_g down to this size scale.

CONCLUSIONS

We have presented experimental evidence that outlines the process by which colloidal silica PNCs are formed when cast from solvents. The colloidal silica is charge stabilized in DMF, regardless of surface treatment. As such, it can be thought of as effective hard spheres diffusing in a viscous liquid. As a formulation dried, the charge colloid structure remained, until about half the solvent had evaporated. After that, the charged double layer collapsed, reducing the surface charge, and hence the effective diameter of the particles. This resulted in increased diffusion of the nanoparticles within the medium, and without the repulsion provided by the charges, they formed clusters. For low molecular weight matrices, these clusters could extend over hundreds of nanometers. When the matrix viscosity was sufficiently high, the diffusive motion was suppressed, and it was possible to produce well-dispersed nanocomposites, where the clusters contain roughly two to four particles. Further study of diffusion-limited aggregation in these systems is underway. These processes may be of interest to researchers in the field who are attempting to create nanocomposites for property measurements. Through the use of DSC measurements, we have also demonstrated that the T_g of these composites is independent of particle loading.

AUTHOR INFORMATION

Corresponding Author
*E-mail: jeff.meth@usa.dupont.com.

ACKNOWLEDGMENT

The authors thank Russ Composto, Karen Winey, and Sangah Gam from the University of Pennsylvania and Nigel Clarke from The University of Sheffield for valuable discussions. We also thank William Wright, Peggy Foster, M. Diane Gedling, Bob Moneta, Ya Liang, and Shahla Ahoorei for technical assistance. Portions of this work were performed at the DuPont–Northwestern–Dow Collaborative Access Team (DND-CAT) located at Sector 5 of the Advanced Photon Source (APS). DND-CAT is supported by E.I. DuPont de Nemours & Co., The Dow Chemical Company, and Northwestern University. Use of the APS, an Office of Science User Facility operated for the U.S. Department of Energy (DOE) Office of Science by Argonne National Laboratory, was supported by the U.S. DOE under Contract DE-AC02-06CH11357.

REFERENCES

(1) Winey, K., Vaia, R., Eds. *Polymer Nanocomposites*; MRS Bulletin; Materials Research Society: Pittsburgh, PA, 2007.
(2) Bhattacharya, S. N.; Gupta, R. K.; Kamal, M. R. *Polymeric Nanocomposites*; Hanser: Cincinnati, OH, 2008.
(3) Jancar, J.; Douglas, J. F.; Starr, F. W.; Kumar, S. K.; Cassagnau, P.; Lesser, A. J.; Sternstein, S. S.; Buehler, M. J. *Polymer* **2010**, *51*, 3321.
(4) Vaia, R. A.; Maguire, J. F. *Chem. Mater.* **2007**, *19*, 2736.
(5) Mackay, M. E.; Tuteja, A.; Duxbury, P. M.; Hawker, C. J.; Van Horn, B.; Guan, Z.; Chen, G.; Krishnan, R. S. *Science* **2006**, *311*, 1740.
(6) Russel, W. B.; Saville, D. A.; Schowalter, W. R. *Colloidal Dispersions*; Cambridge University Press: Cambridge, UK, 1989.
(7) Gapinski, J.; Patkowski, A.; Banchio, A. J.; Buitenhuis, J.; Holmqvist, P.; Lettinga, M. P.; Meier, G.; Nagele, G. *J. Chem. Phys.* **2009**, *130*, 084503.
(8) Gapinski, J.; Patkowski, A.; Nagele, G. *J. Chem. Phys.* **2010**, *132*, 054510.
(9) Gillespie, R. J.; Birchall, T. *Can. J. Chem.* **1963**, *41*, 148.
(10) Carotenuto, G.; Nicolais, L.; Kuang, X.; Zhu, Z. *Appl. Compos. Mater.* **1995**, *2*, 385.
(11) Mauger, M.; Dubault, A.; Halary, J. L. *Polym. Int.* **2004**, *53*, 378.
(12) Mauger, M.; Dubault, A.; Halary, J. L. *J. Mater. Sci.* **2006**, *41*, 8284.
(13) Mauger, M.; Dubault, A.; Halary, J. L. *Polym. Int.* **2007**, *56*, 214.
(14) Ackora, P.; Kumar, S. K.; Sakai, V. G.; Li, Y.; Benicewicz, B. C.; Schadler, L. S. *Macromolecules* **2010**, *43*, 8275.
(15) Etienne, S.; Becker, C.; Ruch, D.; Grignard, B.; Cartigny, G.; Detrembleur, C.; Calberg, C.; Jerome, R. *J. Therm. Anal. Calorim.* **2007**, *87*, 101.
(16) Hub, C.; Harton, S. E.; Hunt, M. A.; Fink, R.; Ade, H. *J. Polym. Sci., Part B: Polym. Phys.* **2007**, *45*, 2270.
(17) Munstedt, H.; Koppl, T.; Triebel, C. *Polymer* **2010**, *51*, 185.
(18) Sen, S.; Xie, Y.; Kumar, S. K.; Yang, H.; Bansal, A.; Ho, D. L.; Hall, L.; Hooper, J. B.; Schweizer, K. S. *Phys. Rev. Lett.* **2007**, *98*, 128302.
(19) Akcora, P.; Liu, H.; Kumar, S. K.; Moll, J.; Li, Y.; Benicewicz, B. C.; Schadler, L. S.; Acehan, D.; Panagiotopoulos, A. Z.; Pryamitsyn, V.; Ganesan, V.; Ilavsky, J.; Thiyagarajan, P.; Colby, R. H.; Douglas, J. F. *Nature Mater.* **2009**, *8*, 354.
(20) Jouault, N.; Vallat, P.; Dalmas, F.; Said, S.; Jestin, J.; Boue, F. *Macromolecules* **2009**, *42*, 2031.
(21) Bogoslovov, R. B.; Roland, C. M.; Ellis, A. R.; Randall, A. M.; Robertson, C. G. *Macromolecules* **2008**, *41*, 1289.
(22) Harton, S. E.; Kumar, S. K.; Yang, H.; Koga, T.; Hicks, K.; Lee, H.; Mijovic, J.; Liu, M.; Vallery, R. S.; Gidley, D. W. *Macromolecules* **2010**, *43*, 3415.
(23) Roy, M.; Nelson, J. K.; MacCrone, R. K.; Schadler, L. S. *J. Mater. Sci.* **2007**, *42*, 3789.
(24) Hall, L. M.; Anderson, B. J.; Zukoski, C. F.; Schweizer, K. S. *Macromolecules* **2009**, *42*, 8435.
(25) Kosmulski, M. *Surfactant Sci. Ser.* **2000**, *90*, 343.
(26) Wiersema, P. H.; Loeb, A. L.; Overbeek, J. T. G. *J. Colloid Interface Sci.* **1966**, *22*, 78.
(27) Ingham, B.; Li, H.; Allen, E. L.; Toney, M. F. *J. Appl. Crystallogr.* **2008**.
(28) Evans, M.; Hastings, N.; Peacock, B. *Statistical Distributions*; Wiley: New York, 2000; p 129.
(29) Qiu, D.; Cosgrove, T.; Howe, A. M.; Dreiss, C. A. *Langmuir* **2006**, *22*, 546.
(30) Hayter, J. B.; Penfold, J. *Mol. Phys.* **1981**, *42*, 109.
(31) German, R. M. *Particle Packing Characteristics*; Metal Powders Industry Federation: Princeton, NJ, 1989.
(32) Lide, D. R. L., Ed. *CRC Handbook of Chemistry & Physics*, 75th ed.; CRC Press: Boca Raton, FL, 1994; pp 6–77.
(33) Gam, S.; Meth, J. S.; Zane, S. G.; Chi, C.; Wood, B. A.; Seitz, M. E.; Winey, K. I.; Clarke, N.; Composto, R. J. *Macromolecules* **2011**, *44*, 3494.
(34) Poon, W. C. K. *J. Phys.: Condens. Matter* **2002**, *14*, R859.
(35) Mutch, K. J.; van Duijneveldt, J. S.; Eastoe *J. Soft Matter* **2007**, *3*, 155.
(36) Fleer, G. J.; Tuinier, R. *Adv. Colloid Interface Sci.* **2008**, *143*, 1.
(37) Fuchs, M.; Schweizer, K. S. *J. Phys.: Condens. Matter* **2002**, *14*, R239.
(38) Hooper, J. B.; Schweizer, K. S.; Desai, T. G.; Koshy, R.; Keblinski, P. *J. Chem. Phys.* **2004**, *121*, 6986.
(39) Hooper, J. B.; Schweizer, K. S. *Macromolecules* **2005**, *38*, 8858.
(40) Hooper, J. B.; Schweizer, K. S. *Macromolecules* **2006**, *39*, 5133.
(41) Hooper, J. B.; Schweizer, K. S. *Macromolecules* **2007**, *40*, 6998.
(42) Bansal, A.; Yang, H.; Li, C.; Cho, K.; Benicewicz, B. C.; Kumar, S. K.; Schadler, L. S. *Nature Mater.* **2005**, *4*, 693.
(43) Speedy, R. J.; Reiss, H. *Mol. Phys.* **1991**, *72*, 999.
(44) Speedy, R. J.; Reiss, H. *Mol. Phys.* **1991**, *72*, 1015.
(45) Bowles, R. K.; Speedy, R. J. *Mol. Phys.* **1994**, *83*, 113.